Available online at www.sciencedirect.com
SCIENCE DIRECT
Polymer 46 (2005) 11744–11754
polymer
www.elsevier.com/locate/polymer

Relationship between nanoscale deformation processes and elastic behavior of polyurethane elastomers

Elizabeth M. Christenson[a,b], James M. Anderson[b,c], Anne Hiltner[a,b,*], Eric Baer[a,b]

[a]Center for Applied Polymer Research, Case Western Reserve University, Cleveland, OH 44106, USA
[b]Department of Macromolecular Science, Case Western Reserve University, Cleveland, OH 44106, USA
[c]Department of Biomedical Engineering and Institute of Pathology, Case Western Reserve University, Cleveland, OH 44106, USA

Received 3 June 2005; received in revised form 11 August 2005; accepted 31 August 2005
Available online 11 October 2005

Abstract

The cyclic deformation of two polyurethane elastomers that differed in soft segment content and molecular weight was investigated. The microphase-separated morphology of the polyurethane with higher soft segment content consisted of hard segment domains dispersed in a soft segment matrix. In the polyurethane with lower soft segment content, the hard segment domains appeared to be partially cocontinuous. Following an initial 'conditioning' cycle, both polyurethanes exhibited reversible elastomeric behavior. Structural changes that occurred during conditioning were investigated using atomic force microscopy and Fourier transform infrared dichroism. The results provided the basis of a structural model for the deformation behavior. Yielding and reorganization of hard domains resulted in a highly oriented microfibrous morphology. Subsequent unloading and reloading were associated with reversible relaxation and reformation of the microfibrous entities. The elastic behavior of the conditioned polyurethanes was satisfactorily described by classical rubber theory with inextensibility. The structural model proposed here extended previous efforts to describe the deformation processes of polyurethanes during cyclic loading.

Keywords: Polyurethanes; Atomic force microscopy; Elastomer

1. Introduction

Thermoplastic elastomers have received considerable attention in recent years due to their combination of elastomeric properties and thermoplastic processing conditions [1]. Unlike traditional elastomers, which derive their elasticity from an amorphous network interconnected by chemical crosslinks, thermoplastic elastomers possess thermoreversible crosslinks. Upon heating or dissolution, the physical crosslinks breakup so that the material flows and can be easily processed. Segmented polyurethanes are one family of commercially important thermoplastic elastomers that possesses a blocky chain structure consisting of hard and soft segments. The hard segment has a high glass transition temperature (T_g) and is typically an aromatic diisocyanate chain extended with a low molecular weight diol or diamine. Common soft segments include polyethers, polyesters and polyalkyl glycols with T_g in the range of -70 to -30 °C.

The thermodynamic incompatibility of the polyurethane hard and soft segments drives microphase separation into semicrystalline hard segment domains that are stabilized by hydrogen bonding between urethane and urea groups [2–4], and amorphous, rubbery soft segment domains. Phase separation improves as the soft segment molecular weight increases [5], and also depends on the hard and soft segments chemistries [6,7], and the process history [8]. For polyurethanes with very good phase separation, larger scale, spherulitic-like organization of the lamellar hard domains is possible [7,9]. Compositions with lower hard segment content consist of hard segment domains dispersed in the soft segment amorphous matrix. The hard domains serve as physical crosslinks and also as reinforcement to the soft segment matrix. With higher hard segment content, hard domain interconnectivity produces continuous, rather than discrete, hard domains [10]. The change in morphology corresponds to a transition in the deformation behavior [11].

The microphase-separated morphology of polyurethanes is responsible for the mechanical properties. The proposed deformation models derive primarily from infrared dichroism

* Corresponding author. Address: Department of Macromolecular Science, Case Western Reserve University, Cleveland, OH 44106, USA.
E-mail address: pah6@po.cwru.edu (A. Hiltner).

0032-3861/$ - see front matter © 2005 Elsevier Ltd. All rights reserved.
doi:10.1016/j.polymer.2005.08.083

of characteristic hard segment and soft segment bands, supplemented by wide angle and small angle X-ray diffraction, transmission electron microscopy, and more recently, by atomic force microscopy [12]. The initial response to stress is elastomeric stretching of the soft segment matrix. Good connection between soft and hard segments due to covalent bonding can cause the hard domains to rotate as rigid units into the strain direction. At a critical strain, the hard domains shear yield. Restructuring, rather than disintegration, of the hard domains is indicted by conservation of hard segment hydrogen bonding [13]. Some irreversible deformation of the hard domains during the first loading is responsible for hysteresis in the stress–strain response and the strain-softening that is typically observed when a polyurethane is restretched [14,15]. This deformation concept has been amenable to constitutive modeling that considers a composite series arrangement of hard and soft domains [16]. Another feature of elastomeric behavior that occurs upon stretching some polyurethanes is strain-crystallization of the soft segments, which is marked by an increase in the stress response [17,18]. After the stress is removed, the crystals melt as the strain recovers. Strain-crystallization can be enhanced by increasing the molecular weight of the soft segment [19].

The nature of hard domain restructuring during deformation continues to be a subject of research. Atomic force microscopy now makes it possible to view the microphase-separated morphologies of polyurethanes, and offers the opportunity to observe directly the morphological changes during deformation. For example, AFM images reveal a fibrillar morphology when a segmented thermoplastic elastomer of PTMO and an aromatic polyamide is highly stretched [20]. The present study compares the solid-state structure and cyclic deformation behavior of two polyurethane elastomers that have the same soft segment chemistry, but differ in soft segment molecular weight and soft segment content. In order to further elucidate the deformation mechanisms of the microphase-separated morphology, and particularly the role of the hard domains, the polyurethanes are examined by atomic force microscopy and other techniques that probe morphology and chain orientation.

2. Materials and methods

2.1. Materials

The chemical structures of the polyurethanes used in this study are shown in Fig. 1 and their physical properties are presented in Table 1. The poly(etherurethane urea) (PEUU) was described previously [21]. It had a poly(tetramethylene oxide) (PTMO) soft segment ($M_n = 2000$ g mol^{-1}) and a di(*p*-phenyl isocyanate) (MDI) hard segment chain extended with mixed diamines. The PEUU was provided as a solution in dimethyl acetamide (DMAC) with concentration of 20% solids by weight. The PEUU solution was cast onto a glass substrate to a uniform thickness using a doctor blade. The solvent was removed in vacuo at ambient temperature. The dried PEUU film had a final thickness of approximately 220 μm. All experiments on PEUU were conducted on cast films.

Elasthane™ 80A (PEU) is a poly(ether urethane) with PTMO soft segment ($M_n = 1000$ g mol^{-1}) and MDI hard segment chain extended with butanediol (BD). The PEU was synthesized by The Polymer Technology Group, Inc. (Berkeley, CA), and was extruded into films by Medtronic, Inc. (Minneapolis, MN) using a Randcastle extruder. Films were extruded onto a chill roll to a thickness of approximately 250 μm. All the materials were synthesized and extruded without additives. For some experiments, the extruded PEU film was dissolved in DMAC and cast into films. The study also included a polyurethane identified as PEUX which had an EO/PO soft segment and about the same soft segment molecular weight as PEUU but similar hard-to-soft segment ratio as PEU. Films of PEUX were cast from DMAC solution.

Relative soft segment concentrations were estimated with attenuated total reflectance Fourier transform infrared (ATR–FTIR) spectroscopy. Data were collected with a Nexus 870 FTIR bench coupled to a Continuum microscope (Thermo

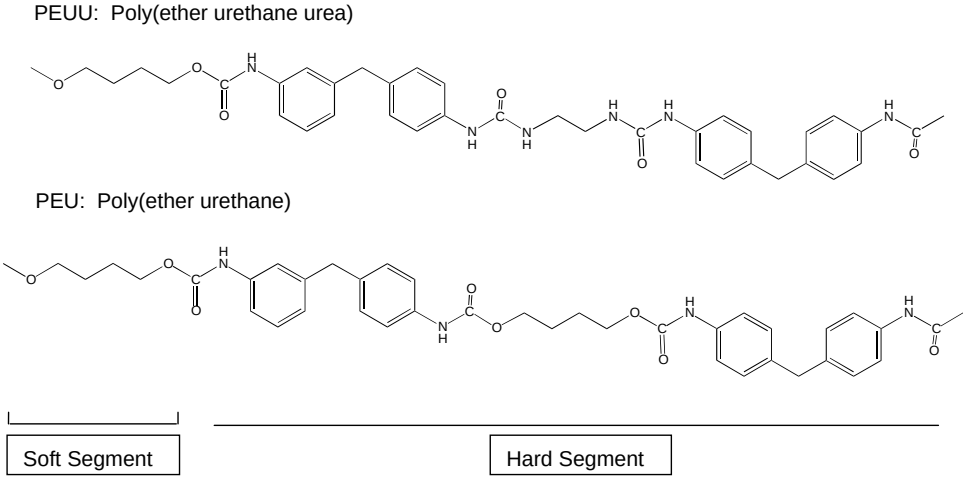

Fig. 1. Chemical structure of polyurethanes.

Table 1
Characterization of polyurethanes

Material		Soft segment	Hard segment	PTMO/MDI[a]	Molecular weight	SS MW
PEUU	Poly(ether urethane urea)	PTMO	MDI/ED	14.0±0.5	75,000	2000
PEU	Elasthane™ 80A	PTMO	MDI/BD	3.8±0.1	225,000	1000
PEUX	Experimental poly(ether urethane)	EO/PO	MDI/BD	4.6±0.1	–	2000

PTMO, poly(tetramethylene oxide); EO, ethylene oxide; PO, propylene oxide; MDI, methylene di(*p*-phenyl isocyanate); BD, butane diol; ED, mixed ethylene diamines; SS MW, soft segment molecular weight.
[a] ATR-FTIR peak height ratio of 1110 cm^{-1} C–O–C soft segment ether peak to 1591 cm^{-1} C=O hard segment carbonyl peak; $n=10$, average ± standard deviation.

Nicolet, Madison, WI). The microscope utilized an attenuated total reflectance (ATR) slide-on attachment with a germanium crystal. Spectra were collected at a resolution of 2 cm^{-1} for 32 scans with a sampling area of 150 μm × 150 μm. Multiple spectra were collected on each polyurethane surface. The ether index was calculated from the peak height of the amorphous aliphatic ether absorbance at 1110 cm^{-1} normalized to the hard segment aromatic carbon–carbon stretch at 1591 cm^{-1}. Normalizing the ATR-FTIR peak heights provided a relative measurement of the soft-to-hard segment ratio, Table 1.

2.2. Material characterization

Dynamic mechanical thermal analysis (DMTA) was performed on polyurethane films with a DMTA MkII unit (Polymer Laboratories, Inc.) operating in the tensile mode. The relaxation spectrum was scanned from −60 to 100 °C with a frequency of 1 Hz and a heating rate of 3 °C min^{-1}.

Engineering stress–strain measurements were performed on an Instron Mechanical Testing instrument (Minneapolis, MN) using the ASTM 1708-D microtensile specimen geometry. The ultimate properties are given in Table 2. Other specimens were cyclically loaded and unloaded in uniaxial tension at ambient temperature at a strain rate of 100% min^{-1} based on the initial gauge length. The specimens were, allowed to recover for 24 h, and reloaded to the same crosshead displacement at the same crosshead speed. Subsequent cycles were conducted following the same procedure.

Atomic force microscopy (AFM) was conducted on unstrained and strained films in air at ambient conditions using the Nanoscope IIIa multimode head from Digital Instruments (Santa Barbara, CA). Strained specimens were imaged using a special specimen holder to maintain the stretched state. Experiments were conducted in the tapping mode using Si probes with a 60 N m^{-1} spring constant, approximately 10 nm radius, and resonance frequencies in the range of 284–362 kHz. The films were rinsed with acetone and allowed to air dry prior to imaging. Phase and height images were collected simultaneously. Imaging values of the free oscillation amplitude (A_o) and the set point amplitude (A_{sp}) were recorded for each image. Free oscillation amplitude (A_o) and set point ratio (A_{sp}/A_o) are reported for each image to distinguish between tapping conditions. Comparisons among materials were made on phase images obtained with similar tapping conditions, A_o = 15–20 nm and A_{sp}/A_o = 0.80–0.90.

Table 2
Mechanical properties of polyurethanes

Material	2% secant modulus (MPa)	Fracture strain (%)	Fracture stress (MPa)
PEUU	13±1	731	43
PEU	27±2	575	52
PEUX	17±2	–	–

$n=3$, average ± standard deviation.

Films for infrared dichroism experiments were cast onto a glass substrate from a 1 wt% solution in DMAC. The solvent was removed in vacuo at ambient temperature. The dried films had final thickness of 5–10 μm. Infrared spectra of stretched specimens were obtained with a stretching device mounted in the sample chamber of a Nicolet 870 FTIR spectrometer. Multiple spectra of strained films were collected in the transmission mode at a resolution of 2 cm^{-1} for 32 scans. Spectra were collected with polarization parallel and perpendicular to the stretching direction.

The orientation function of stretched films was calculated from the infrared dichroism using established techniques [11,12,17]. The soft segment orientation was determined from the peak height of the 2940 cm^{-1} CH_2 asymmetric stretching vibration with local baselines. The hard segment orientation was obtained from the carbonyl band at 1709 cm^{-1}. The second moment of the orientation function (P_2) was calculated as

$$P_2 = \left[\frac{(R_o+2)(R-1)}{(R_o-1)(R+2)}\right] \quad (1)$$

where $R = A_{\parallel}/A_{\perp}$ is the measured dichroic ratio of the peak intensities, and R_o is the dichroic ratio for perfect orientation given by $R_o = 2\cot^2\theta$, where θ is the angle between the transition dipole moment and the local chain segment axis. The values of θ for the CH_2 and the carbonyl stretching bands were 90 and 78°, respectively [17].

3. Results and discussion

3.1. Mechanical response

The dynamic mechanical relaxation behavior of the two polyurethanes, PEUU and PEU, is shown in Fig. 2. The glass transition temperature (T_g) was identified by a drop in storage modulus (E') and prominent peaks in tan δ and in loss modulus

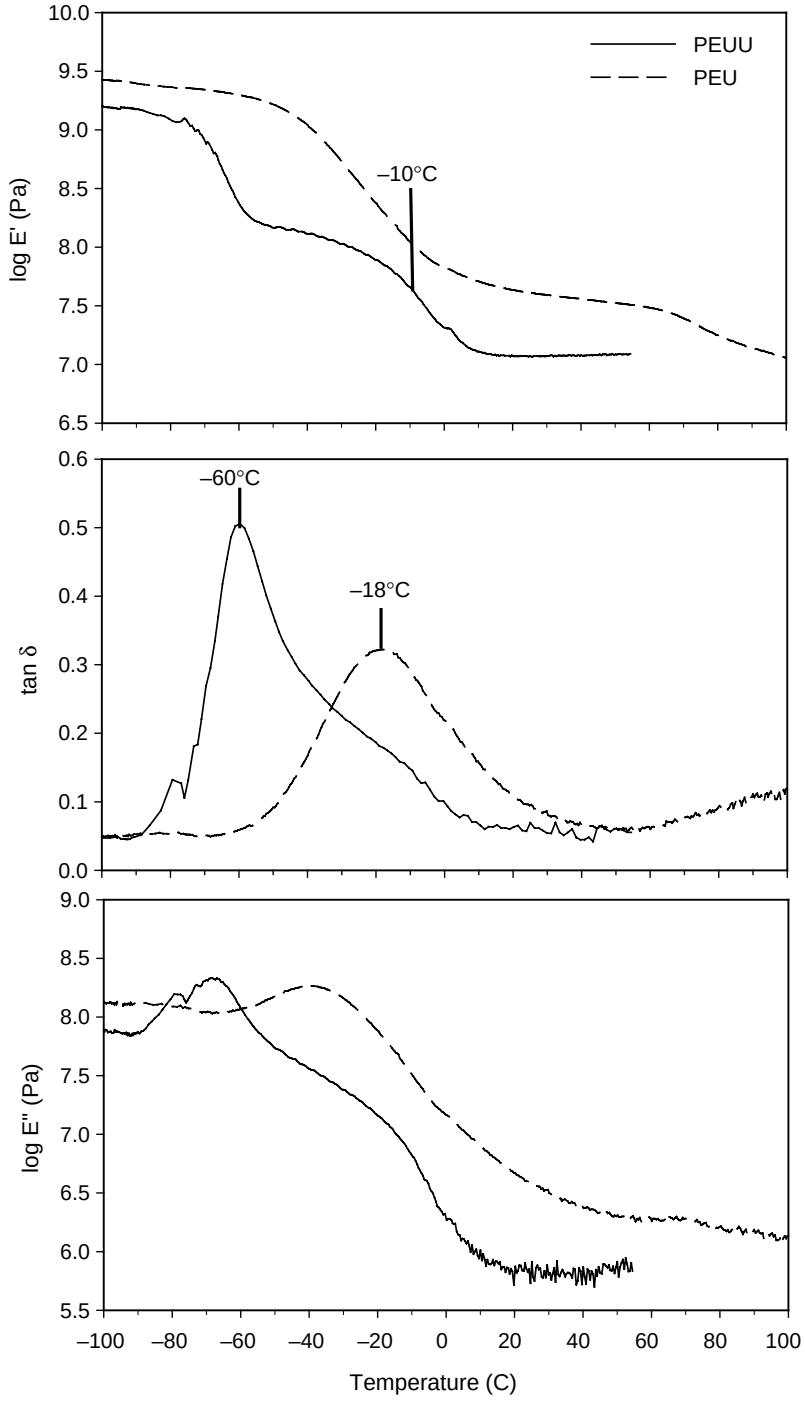

Fig. 2. Dynamic mechanical relaxation behavior of PEUU and PEU.

(E''). The glass transition was associated with onset of soft segment mobility. Considerably higher T_g of PEU (−18 °C) compared to PEUU (−60 °C) was attributed to greater constraint on PEU soft segments, which resulted from the shorter length of PEU soft segments and the higher concentration of constraining hard segments. A second transition at −10 °C appeared in the spectra of PEUU as a smaller drop in the E' curve and as shoulders on the tan δ and E'' curves. The transition temperature was consistent with the reported melting temperature of PTMO [19]. Absence of this transition in the PEU spectrum indicated that constraint on the soft segments effectively prevented their crystallization.

The stress–strain behavior of PEUU and PEU was typical of elastomers with low initial modulus, uniform extension to high strains, and high recovery. The cyclic stress–strain behavior of PEUU loaded to 600% strain and for PEU loaded to 500% strain is shown in Fig. 3. The solid lines represent the initial 'conditioning' loading/unloading cycle. The loading curve shows an initial modulus region followed by a plateau of almost constant stress and strain hardening at higher strains.

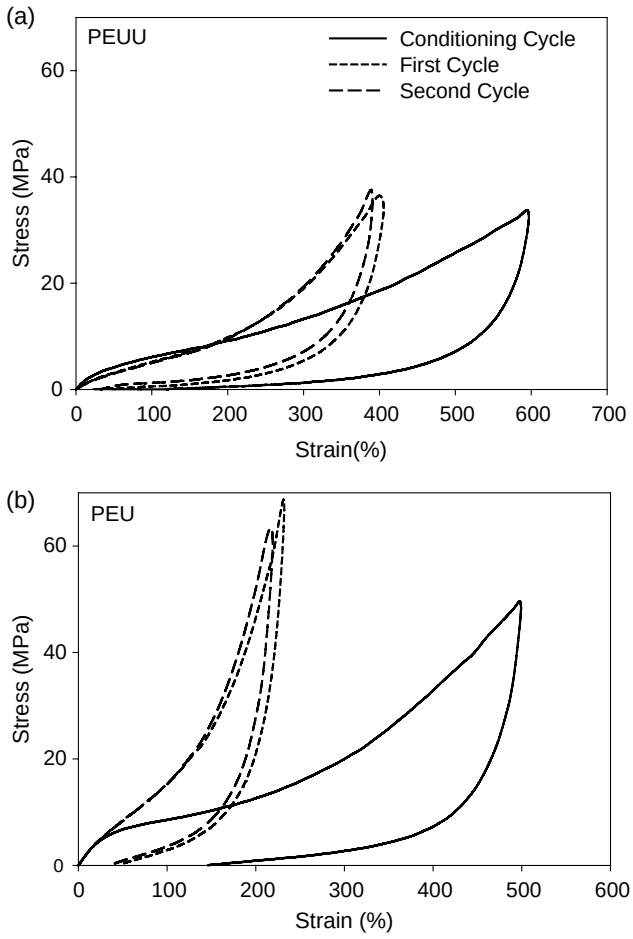

Fig. 3. The initial 'conditioning' loading and unloading cycle and the two subsequent cycles: (a) PEUU for a conditioning strain of 600%; and (b) PEU for a conditioning strain of 500%.

Compared to PEUU, the PEU curve was characterized by a higher initial modulus, a more pronounced knee at the beginning of the plateau region, and the onset of strain hardening at a lower strain. These differences were consistent with the higher hard segment content and the more highly constrained soft segments of PEU. Although PEU was stretched to a lower strain, the amount of permanent set after the load was released was higher for PEU than for PEUU, 143% compared to 103%.

Reloading to the initial extension produced a different stress–strain response, however, additional reloading cycles produced almost no further change. Because of the permanent set after the initial loading, the reloaded specimens had longer gauge length and smaller cross-sectional area. The stress and strain response for the reloading cycles in Fig. 3 was calculated from the new specimen dimensions. After the initial loading, the materials exhibited essentially reversible deformation. Thus, during the initial conditioning loading, the material underwent permanent structural changes. The new structure exhibited reversible behavior on subsequent reloading cycles if the initial extension was not exceeded.

The effect of conditioning strain on the permanent set of PEU and PEUU is compared in Fig. 4. For PEUU,

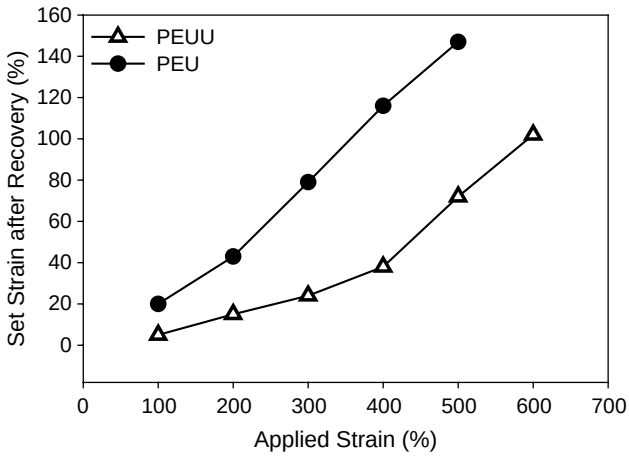

Fig. 4. Set strain after recovery from the conditioning cycle of polyurethanes as a function of conditioning strain.

the permanent set showed a linear dependence for strains up to about 400%, followed by stronger strain dependence between 400 and 600%. The permanent set was much larger for PEU, and increased almost linearly with the conditioning strain.

3.2. Microstructure deformation

The structural changes that occurred during conditioning were probed by AFM. Unstrained PEUU exhibited a two-phase morphology in AFM phase images, Fig. 5(a). The dark matrix of lower modulus corresponded to the soft segments and the brighter dispersed domains of higher modulus corresponded to the hard segments. The hard segment domains were 5–10 nm thick and some were up to 100 nm in length. Stretching PEUU to 100% strain resulted in some breakup of the hard domains, Fig. 5(b). At 200% strain, the broken hard domains started to reassemble into stacks, Fig. 5(c), and at 500% strain the stacks became fibrils that were extended in the stretching direction, Fig. 5(d).

When the stress was released, the oriented fibril morphology of PEUU was lost, and was replaced with an essentially unoriented dispersion of irregular hard domains, Fig. 5(e). Although the fibrous texture was lost, the original morphology was not recovered. Hard segment domains were shorter and less well-organized than originally (compare Fig. 5(e) with Fig. 5(a)). Upon restretching, a fibrous morphology reappeared that was essentially indistinguishable from the fibrous morphology obtained on the conditioning cycle, Fig. 5(f).

The AFM phase image of unstretched PEU showed a higher fraction of bright hard domains, which was consistent with the higher hard segment content, Fig. 6(a). The long, thin domains that characterized the PEUU images were not present, instead the PEU hard segments formed interconnected short domains that suggested a partially cocontinuous morphology. During stretching of PEU, similar processes of hard domain breakup, yielding and fibril formation occurred as in PEUU, although the various processes occurred at lower strains. Fibrils formed at 400% strain were thicker and more densely arrayed than those of PEUU, Fig. 6(b).

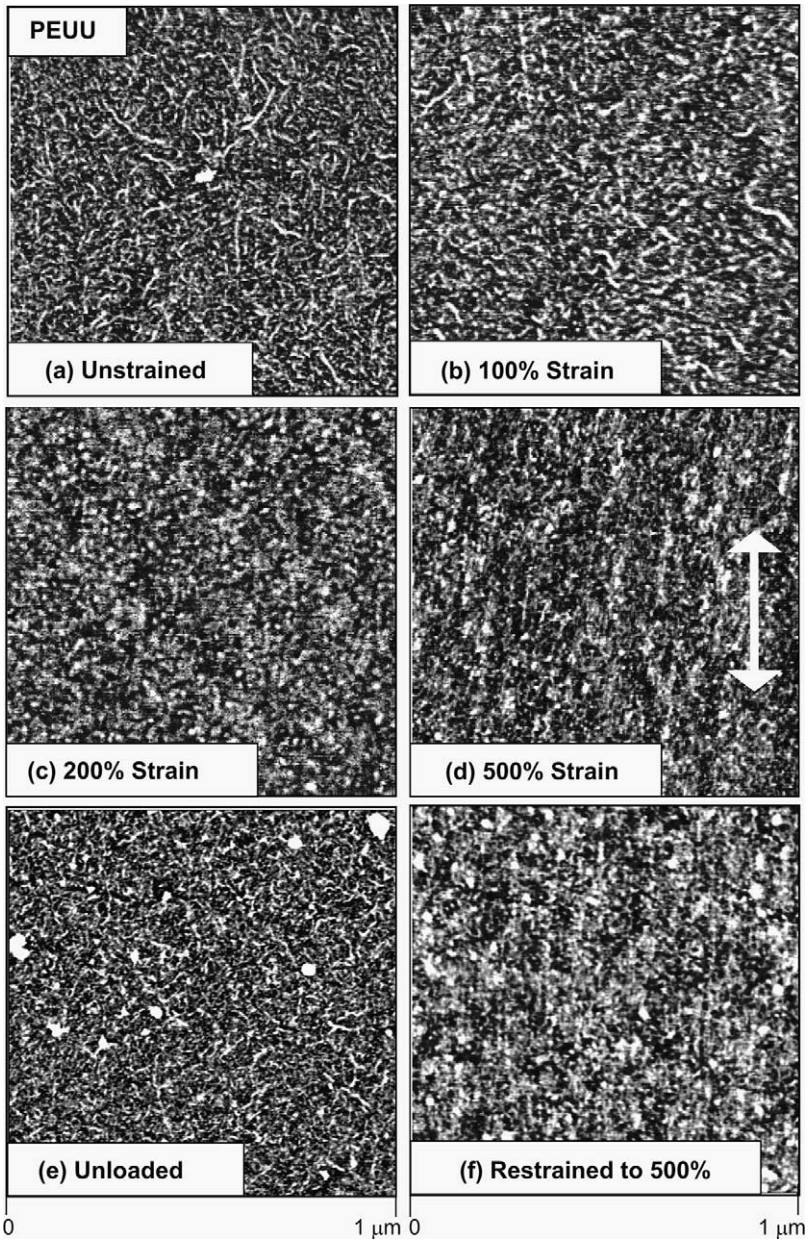

Fig. 5. AFM phase images of PEUU: (a) unstrained; (b) at 100% conditioning strain; (c) at 200% strain; (d) at 500% strain; (e) unloaded; and (f) restrained to 500%. The arrow indicates the stretch direction. $A_o = 20–30$ nm, $A_s/A_o = 0.80–0.90$.

Molecular orientation of hard and soft segments during stretching was obtained from infrared dichroism as shown in Fig. 7. Hard and soft segments of PEUU showed the same gradual increase in orientation to 300% strain. Above 300% strain, orientation increased more rapidly with somewhat higher soft segment orientation. When the stress was removed, the soft segments recovered completely whereas the hard segments showed some level of residual orientation.

Compared to PEUU, stretched PEU exhibited much higher levels of orientation in both the hard and soft segments (note the difference in scale between Fig. 7(a) and (b)). Soft segment orientation increased almost linearly with strain. The hard segments were less well-oriented than the soft segments, especially at higher strains. Both soft and hard segments retained some amount of orientation after the stress was removed, with higher residual orientation in the hard segments.

Crystallization of PEUU soft segments was indicated by dynamic mechanical measurements. Although the melting point was sub-ambient, the possibility existed that stretching induced some amount of soft segment crystallization at ambient temperature. The most distinctive indication of crystallization was a band at 996 cm^{-1} in the infrared spectrum [22]. The effect of strain on this region of the infrared spectrum of PEU and PEUU is shown in Fig. 8. A small crystalline peak at 996 cm^{-1} appeared in the PEUU spectrum at 200% strain, which coincided with the onset of strain hardening in the stress–strain curve. The pronounced increase in peak height as the strain increased further into the strain hardening region

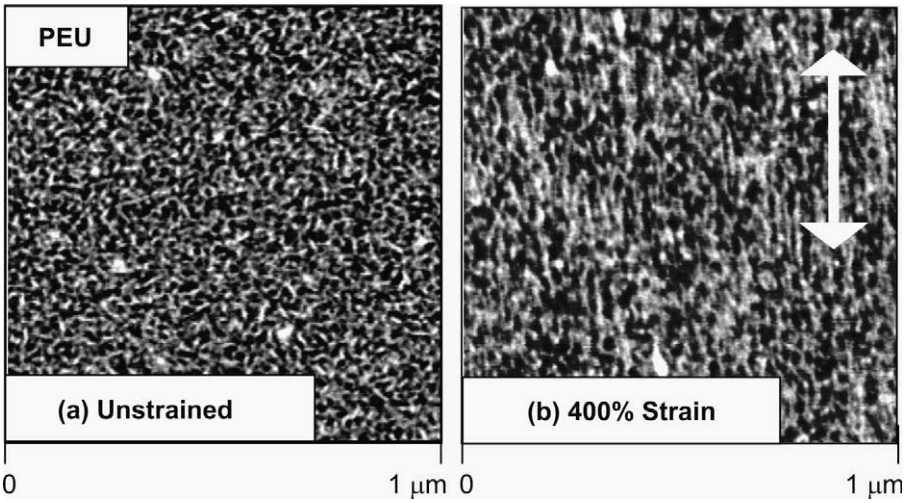

Fig. 6. AFM phase images of PEU: (a) unstrained; and (b) at 400% conditioning strain. The arrow indicates the stretch direction. $A_o = 20–30$ nm, $A_s/A_o = 0.80–0.90$.

suggested that strain-induced crystallization of the soft segment contributed to strain hardening in PEUU.

In contrast, the PEU soft segments did not readily strain-crystallize. A small band at 993 cm^{-1} indicated some crystallization at the highest strain. To quantify the amount of crystallization, the crystalline peak height at 500% strain was normalized to the aromatic reference peak at 1591 cm^{-1}. The normalized peak height was considerably smaller for PEU than for PEUU, 0.35 compared to 1.40. Decreased strain-induced crystallization was consistent with the high level of constraint on PEU soft segments.

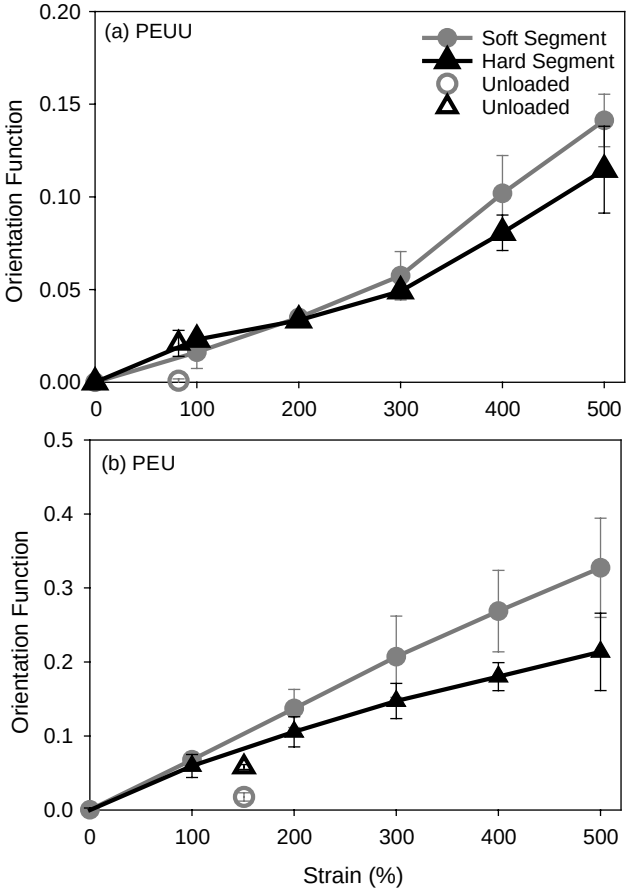

Fig. 7. Soft segment and hard segment orientation as a function of conditioning strain: (a) PEUU; and (b) PEU. ($n = 3$)

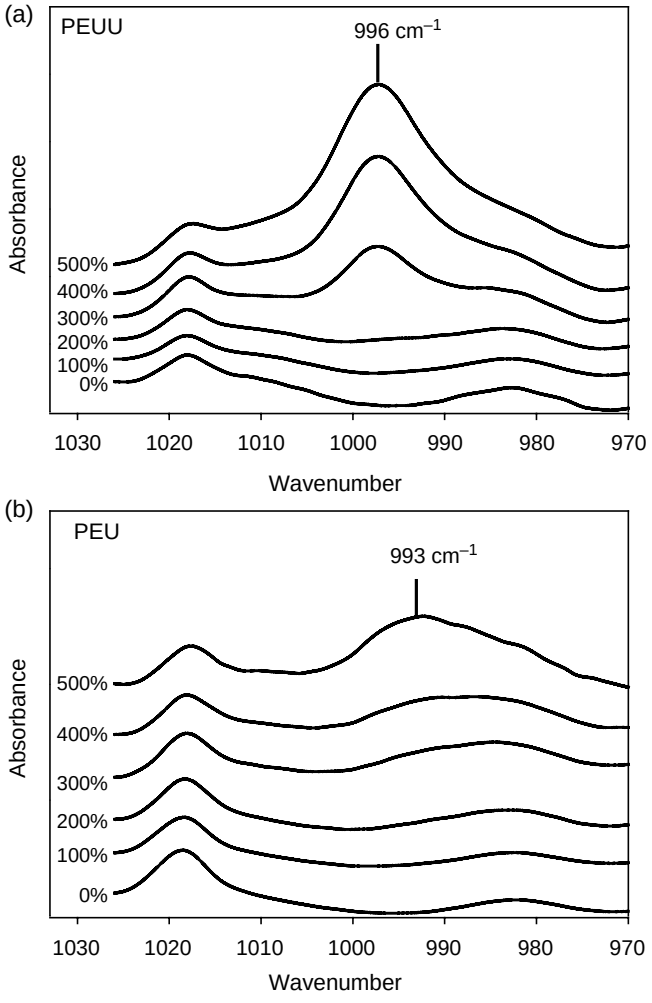

Fig. 8. Strain induced crystallization of PEU and PEUU as indicated by the PTMO crystal band at 996 cm^{-1}: (a) PEUU; and (b) PEU.

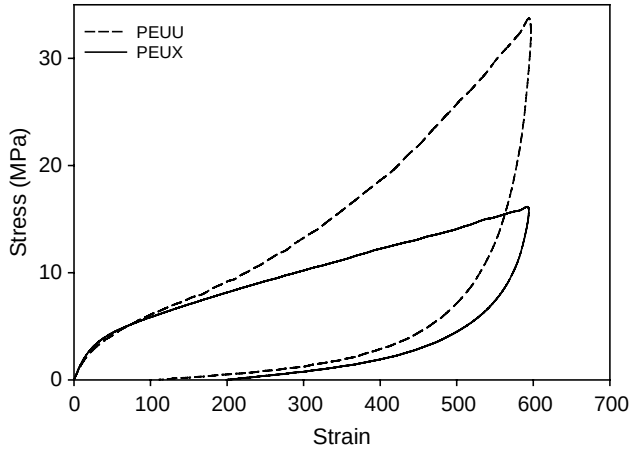

Fig. 9. Comparison of the conditioning cycle stress–strain curves of PEUU and PEUX.

The possibility that strain-induced crystallization contributed to strain hardening of PEUU was tested using a polyurethane with a non-crystallizable EO/PO soft segment, PEUX. This polyurethane had about the same soft segment molecular weight as PEUU (2000 g mol^{-1}) but similar hard-to-soft segment ratio to PEU. The conditioning stress–strain curves of PEUX and PEUU are compared in Fig. 9. The initial stress response of PEUX overlapped that of PEUU as this region of the stress–strain curve depends mainly on soft segment extension. However, at higher strain, PEUX did not exhibit the stress rise that was characteristic of strain hardening.

Considering the low level of soft segment crystallization of PEU, it appeared that the strong strain hardening response of PEU was associated with elastic constraint on the short soft segment matrix and plastic deformation of the partially cocontinuous hard domains. Plastic deformation resulted in a high level of molecular orientation as observed in IR dichroism measurements. The dispersed hard segment domains of PEUU were also plastically deformed as a result of good connectivity to the soft segment matrix. However, in the case of PEUU, it appeared that soft segment crystallization contributed as well to the strain-hardening.

3.3. Deformation model

A discussion of the structural changes that accompany deformation first considers PEUU. The unstretched PEUU consists of hard segment domains dispersed in an elastomeric soft segment matrix, Fig. 10(a). In this case, hard segment domains constitute about 24% by weight [21]. Because the hard segment content is fairly low, these domains are assumed to be lamellae with the chain axis perpendicular to the long axis of the domain, rather than fibers with the chain axis parallel to the domain axis [23]. It can be imagined that the initial response to an imposed stress is stretching of the soft segment matrix chains. Good stress transfer to chains in hard segment domains causes the hard domains to breakup at flaws and to rotate into the strain direction, Fig. 10(b). Evidence of hard segment breakup appears in AFM images at 100% strain. Through the plateau region of the stress–strain curve, the processes of soft segment extension and hard segment breakup and yielding result in increasing molecular orientation of soft and hard segments as seen by IR, Fig. 10(c). Connections to extended soft segments cause the hard segments to reform as stacks of small domains oriented in the stretch direction. Strain hardening beginning at about 300% strain coincides with strain crystallization of extended soft segment chains, and is accompanied by a stronger strain dependence of soft and hard segment orientation (Fig. 7(a)), and a stronger strain dependence of the unrecovered strain (Fig. 4). At 500% strain,

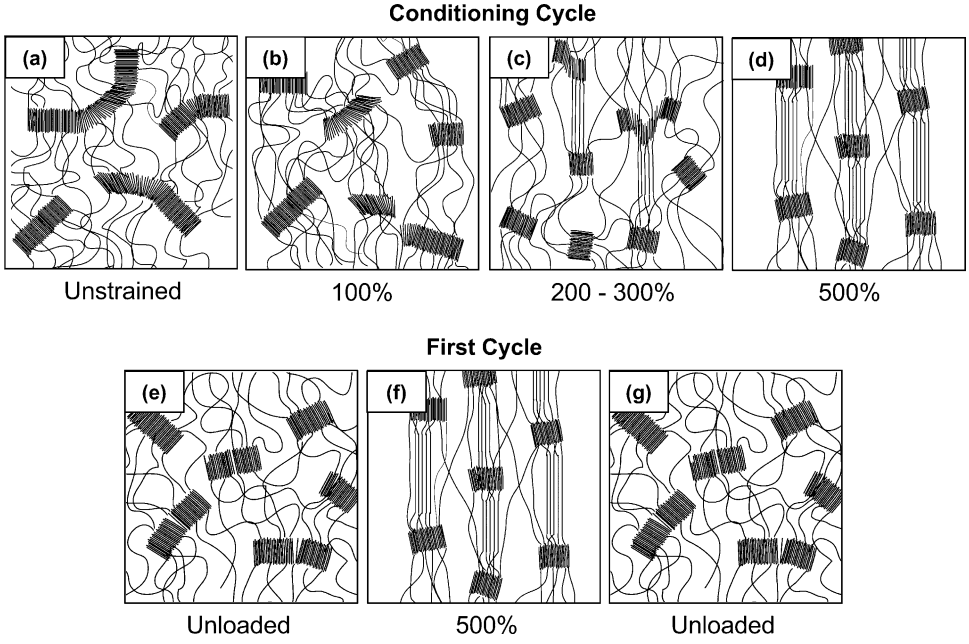

Fig. 10. The proposed structural models for conditioning and reloading of PEUU.

deformation processes result in composite microfibrils consisting of parallel hard and soft segments with small semicrystalline hard domains separated by strain-crystallized soft segment domains, Fig. 10(d). The deformation model is similar to that proposed previously on the basis of IR dichroism and small angle X-ray scattering patterns [23]. Here, the model is confirmed by direct observation with AFM.

Upon removal of the stress, soft segments melt and completely lose their orientation (Fig. 7(a)). With retraction of soft segments, the hard segments lose their fibrous alignment and the original domain morphology reforms to some extent, Fig. 10(e). Some residual orientation of the hard segments is attributed to irreversible deformation of the domains. When reloaded, the stretched soft segment matrix chains realign the hard domains and the microfibril morphology is restored, Fig. 10(f). This process is essentially reversible with virtually no additional irreversible deformation, Fig. 10(g).

Similar structural changes accompany stretching of PEU. However, in this case, hard segment domains constitute about 40% by weight [24], which is close to the composition where the phases become cocontinuous [10,11]. As a consequence, breakup and yielding of hard domains starts at lower strains and results in a higher level of irreversible deformation. Strain induced crystallization does not contribute very much to strain hardening of PEU. Rather, the strong stress response beginning at about 200% strain is attributed to plastic deformation of the partially cocontinuous hard domains and constraints imposed on the relatively short PEU soft segments by attachment to the hard segment domains, as indicated by the high soft segment T_g of PEU.

3.4. Elastomeric behavior

The stress response of PEUU and PEU is presented in Fig. 11 in terms of rubber modulus (G) defined as

$$G = \frac{\sigma}{(\lambda - \lambda^{-2})} \tag{2}$$

where λ is the extension ratio and σ is the engineering stress. In the conditioning cycle, gradually decreasing modulus at low strains is followed by an upswing at high strains. The drop in modulus in the conditioning cycle is attributed to the irreversible breakup of hard domains and loss of physical crosslinks in the elastic network in accordance with the structural model. In contrast, the first and second reloading cycles exhibit almost constant modulus at low strains followed by a strong increase in modulus at high strains. Almost constant modulus on the first and second reloading cycles attests to the stability of the elastic network produced on the conditioning cycle. Overall, the stress response after conditioning closely resembles that of an ideal rubber with inextensibility.

The permanent structure attained on the conditioning cycle provides the polyurethane with elastomeric behavior. The structural model is the basis for analysis according to the classical rubber theory modified for chain inextensibility. The crosslink model describes the elasticity of a crosslink network by considering the additional contributions of finite

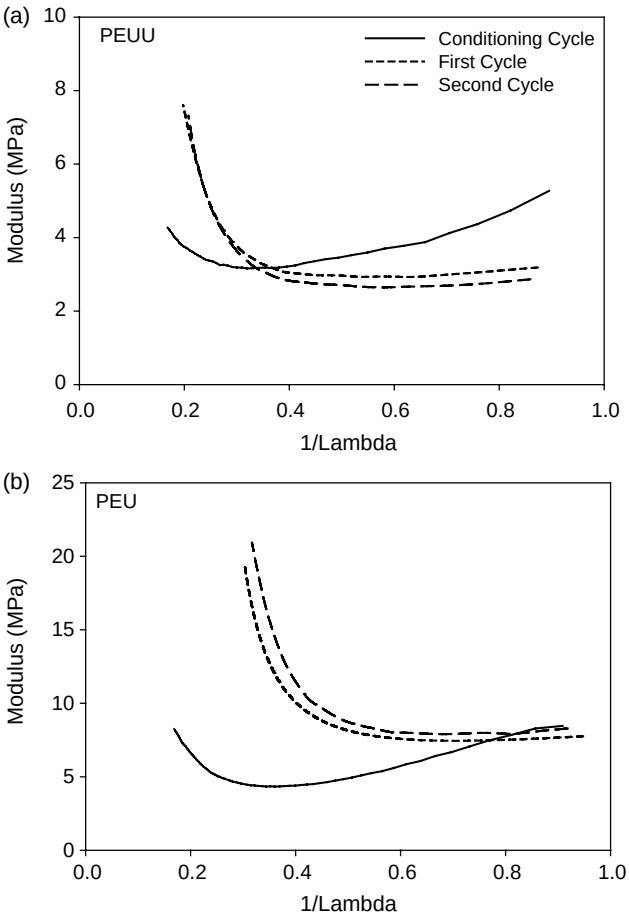

Fig. 11. Rubber modulus of the conditioning, first and second cycle loading curves: (a) PEUU; and (b) PEU.

chain extensibility to the elastic free energy (F) [25,26]

$$\frac{F}{kT} = \frac{1}{2}N_c\left(\frac{\sum_i \lambda_i^2(1-\alpha^2)}{1-\alpha^2\sum_i \lambda_i^2} + \log\left(1-\alpha^2\sum_i \lambda_i^2\right)\right) \tag{3}$$

where N_c is the crosslink density and α is a parameter describing the inextensibility. The summation is performed over three Cartesian components of strain λ. For uniaxial tension, $\lambda_1 = \lambda$ and $\lambda_2 = \lambda_3 = \lambda^{-1/2}$. From the expression for stress

$$\sigma = \left(\frac{\partial F}{\partial \lambda}\right)_{T,V} \tag{4}$$

Eq. (3) gives

$$\sigma = N_c kT\left(\lambda - \frac{1}{\lambda^2}\right)\left(\frac{1-\alpha^2}{(1-\alpha^2\phi)^2} - \frac{\alpha^2}{1-\alpha^2\phi}\right) \tag{5}$$

where σ is the stress, λ is the draw ratio, k is the Boltzmann constant, T is the temperature, N_c is density of crosslinked chains assuming a functionality of four, α is the chain inextensibility, and ϕ is defined as

$$\phi = \lambda^2 + \frac{2}{\lambda} \tag{6}$$

A two parameter least squares fit was performed to obtain α and N_c.

The calculated modulus curves for the first loading curve after the conditioning cycle fit the entire range of deformation very well as shown in Fig. 12. The fit parameters for the first and second loading cycles were essentially the same, Table 3. A higher crosslink density was obtained for PEU than for PEUU, $14\times10^{-26}\,m^{-3}$ compared to $5.7\times10^{-26}\,m^{-3}$. The molecular weight of the chain segment between crosslinks (M_c) was obtained from the crosslink density according to

$$M_c = \frac{\rho N_A}{N_c} \tag{7}$$

where ρ is the density, taken as $1.12\,g\,cm^{-3}$, and N_A is Avogadro's number. As expected, PEUU had larger M_c than PEU by a factor of two, 1000 compared to 500 g mol^{-1}. The values corresponded closely to the soft segment molecular weight of the two polyurethanes, 2000 and 1000 g mol^{-1}. This supported the proposed structural model in which the hard domains acted as network junctions for the extensible soft segments. The somewhat low values of M_c compared to the soft segment molecular weights was attributed to the multi-functionality of the hard domain junctions and the high volume fraction of hard domains.

The inextensibility parameter (α) was higher for PEU than PEUU, 0.201 compared to 0.126. Inextensibility in elastomers has been attributed to finite chain length between immobile junctions [25,26], although in some cases, such as natural rubber, it has been proposed that strain induced crystallization accounts for the observed increase in tensile stress [27]. For PEUU, the factor α included the effect of strain crystallization. In contrast, for PEU, α was thought of as describing the constraint imposed by the partially cocontinuous hard domains on extension of the soft segments.

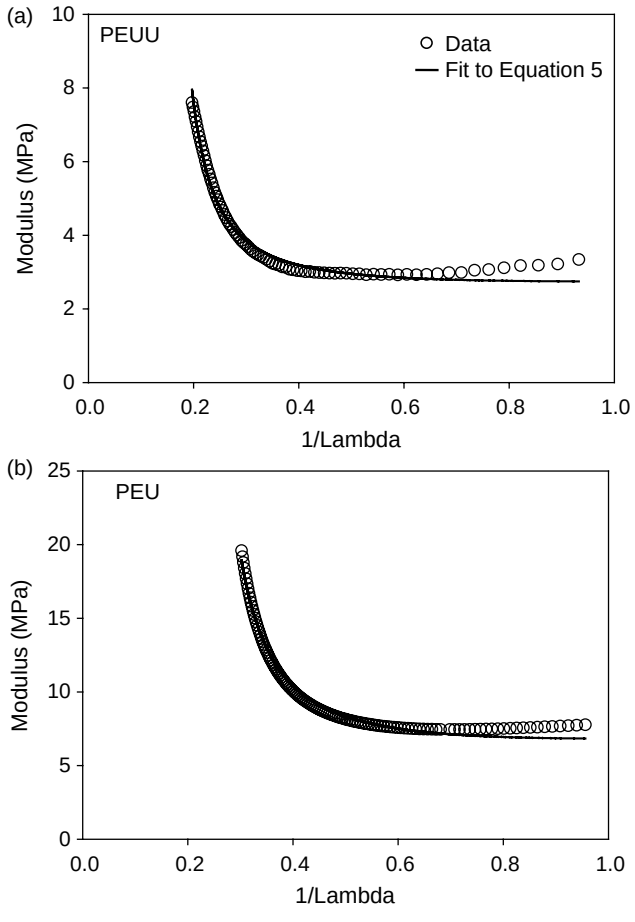

Fig. 12. Fit of Eq. (5) to the first cycle loading curve: (a) PEUU; and (b) PEU.

Table 3
Crosslink model parameters

PEUU	α	N_cKT (MPa)	N_c ($10^{-26}\,m^{-3}$)	M_c (g mol^{-1})
First cycle	0.126±0.004	2.3±0.2	5.7±0.5	1000±100
Second cycle	0.132±0.006	2.3±0.1	5.8±0.4	1000±100
PEU	α	N_cKT (MPa)	N_c ($10^{-26}\,m^{-3}$)	M_c (g mol^{-1})
First cycle	0.201±0.001	5.6±0.7	14±2	500±100
Second cycle	0.220±0.010	5.4±0.7	13±2	500±100

$n=3$, average±standard deviation.

4. Conclusions

This study compared the solid-state structure and cyclic deformation behavior of two polyurethane elastomers with the same soft segment chemistry, but with different soft segment molecular weight and soft segment content. The polyurethanes exhibited a microphase-separated morphology. The morphology of the polyurethane with higher soft segment content consisted of hard segment domains dispersed in a soft segment matrix. In the polyurethane with lower soft segment content, the hard segment domains appeared to be partially cocontinuous. This resulted in an elastomer with higher modulus, stronger strain hardening, and more irreversible deformation.

It was possible to identify the structural changes during loading from direct AFM observation of the microphase-separated morphology. The results confirmed the major features of models proposed previously. Thus, the initial response to stress was elastic stretching of the soft segment matrix. Good connection between soft and hard segments caused the hard domains to breakup and shear yield. The previous studies were extended to reveal a fibrous morphology at high strains. The microfibrils resulted from reorganization of the hard segments into small domains, which were separated by extended soft segment domains.

Upon removal of stress, retraction of soft segments caused the hard segments to lose their fibrous alignment and to reform the original domain morphology to some extent. Residual orientation of the hard segments indicated that there was some irreversible deformation during the initial 'conditioning' cycle that created the microfibrils. When reloaded, stretching of the soft segment matrix chains realigned the hard domains and the microfibrillar morphology was restored. Further cyclic loading was accompanied by reversible relaxation and regeneration of the load-bearing microfibrils.

Irreversible deformation of the hard domains during the first 'conditioning' loading was responsible for strain-softening and hysteresis in the stress–strain response. Following the conditioning cycle, the polyurethanes exhibited reversible elastomeric behavior as long as the initial extension was not exceeded. Classical rubber theory with inextensibility satisfactorily described the elastic behavior of the conditioned polyurethanes. The extracted values of M_c, the molecular weight between network junctions, were comparable to the soft segment molecular weight. This study revealed the structural basis of the elastomeric behavior of polyurethanes and confirmed the significant role of hard segment domains.

Acknowledgements

The authors thank Dr Ben Poon and Dr Christopher Christenson of The Dow Chemical Company for technical assistance. This research was supported by the National Institutes of Health, Grant EB-00272.

References

[1] Legge NR, Holden G, Schroeder HE, editors. Thermoplastic elastomers: a comprehensive review. Munich: Hanser; 1987.
[2] Bonart R. J Macromol Sci Phys 1968;B2:115–38.
[3] Bonart R, Morbitzer L, Hentze G. J Macromol Sci Phys 1969;B3:337–56.
[4] Bonart R, Morbitzer L, Muller EH. J Macromol Sci Phys 1974;B9: 447–61.
[5] O'Sickey MJ, Lawrey BD, Wilkes GL. J Appl Polym Sci 2002;84: 229–43.
[6] Zha L, Wu M, Yang J. J Appl Polym Sci 1999;73:2895–902.
[7] Chang Y-JP, Wilkes GL. J Polym Sci, Polym Phys Ed 1975;13:455–76.
[8] Lee HS, Ko JH, Song KS, Choi KH. J Polym Sci, Part B: Polym Phys 1997;35:1821–32.
[9] Fridman ID, Thomas EL. Polymer 1980;21:388–92.
[10] Martin DJ, Meijs GF, Gunatillake PA, Yozghatlian SP, Renwick GM. J Appl Polym Sci 1999;71:937–52.
[11] Lin SB, Hwang KS, Tsay SY, Cooper SL. Colloid Polym Sci 1985;263: 128–40.
[12] Lee HS, Yoo SR, Seo SW. J Polym Sci, Part B: Polym Phys 1999;37: 3233–45.
[13] Seymour RW, Estes GM, Cooper SL. Macromolecules 1970;3:579–82.
[14] Estes GM, Seymour RW, Cooper SL. Macromolecules 1971;4:452–7.
[15] Puett D. J Polym Sci, Part A-2 1967;5:839–52.
[16] Falabella R, Farris RJ, Coooper SL. J Rheol 1984;28:123–54.
[17] Reynolds N, Spiess HW, Hayen H, Nefzger H, Eisenbach CD. Macromol Chem Phys 1994;195:2855–73.
[18] Wilkes CE, Yusek CS. J Macromol Sci Phys 1973;B7:157–75.
[19] Niesten MCEJ, ten Brinke JW, Gaymans RJ. Polymer 2001;42:1461–9.
[20] Sauer BB, McLean RS, Brill DJ, Londono DJ. J Polym Sci, Part B: Polym Phys 2002;40:1727–40.
[21] Renier M, Wu YK, Anderson JM, Hiltner A, Lodoen GA, Payet CR. J Biomater Sci, Polym Ed 1994;5:511–29.
[22] Schubert MA, Wiggins MJ, Anderson JM, Hiltner A. J Biomed Mater Res 1997;35:319–28.
[23] Yeh F, Hsiao BS, Sauer BB, Michel S, Siesler HW. Macromolecules 2003;36:1940–54.
[24] Wiggins MJ, MacEwan M, Anderson JM, Hiltner A. J Biomed Mater Res 2004;68A:668–83.
[25] Edwards SF, Vilgis Th. Polymer 1986;27:483–92.
[26] Treloar LRG. The physics of rubber elasticity. London: Oxford University Press; 1967.
[27] Ward IM, Hadley DW. An introduction to the mechanical properties of solid polymers. New York: Wiley; 1993 p. 41–42 [chapter 3].